

Epidermal growth factor promotes a mesenchymal over an amoeboid motility of MDA-MB-231 cells embedded within a 3D collagen matrix^{*,**}

Dongil T. Geum¹, Beum Jun Kim¹, Audrey E. Chang², Matthew S. Hall¹, and Mingming Wu^{1,a}

¹ Department of Biological and Environmental Engineering, Cornell University, Ithaca, NY 14853, USA

² Research Apprenticeship in Biological Sciences, Cornell University, Ithaca, NY 14853, USA

Received: 31 August 2015 / Revised: 6 November 2015

Published online: 14 January 2016 – © Società Italiana di Fisica / Springer-Verlag 2016

Abstract. The receptor of epidermal growth factor (EGFR) critically regulates tumor cell invasion and is a potent therapeutic target for treatment of many types of cancers, including carcinomas and glioblastomas. It is known that EGF regulates cell motility when tumor cells are embedded within a 3D biomatrix. However, roles of EGF in modulating tumor cell motility phenotype are largely unknown. In this article, we report that EGF promotes a mesenchymal over an amoeboid motility phenotype using a malignant breast tumor cell line, MDA-MB-231, embedded within a 3D collagen matrix. Amoeboid cells are rounded in shape, while mesenchymal cells are elongated, and their migrations are governed by a distinctly different set of biomolecules. Using single cell tracking analysis, we also show that EGF promotes cell dissemination through a significant increase in cell persistence along with a moderate increase of speed. The increase of persistence is correlated with the increase of the percentage of the mesenchymal cells within the population. Our work reveals a novel role of microenvironmental cue, EGF, in modulating heterogeneity and plasticity of tumor cell motility phenotype. In addition, it suggests a potential visual cue for diagnosing invasive states of breast cancer cells. This work can be easily extended beyond breast cancer cells.

1 Introduction

The receptor of the epidermal growth factor (EGFR) is known to correlate with tumor invasiveness *in vivo* and mammalian cell motility *in vitro* [1–7]. EGF is a potent signaling molecule that modulates speed and persistence of many cell types including keratinocytes [4], fibroblasts [6,8], carcinoma [5,6,9–20], and glioblastoma cells [21]. Most work reported on roles of EGF in cell migration is carried out on a 2D substrate [22] because 2D assay is relatively straightforward to perform. In 2D, cells adhere to the surface via their basal sides and they migrate via a cyclic process including the extension and adhesion of the leading lamellipodia, the contraction of the rear cortex and release of the trailing edge [7,22]. EGF is known to alter cell adhesion to the surface, speed and persistence [8,23,24]. Recently, the rapid advancement of the field of biomaterials enabled us to investigate cell migration in a more physiologically realistic setting, a 3D biomatrix. Meyer *et al.* and others demonstrated that tumor cell motility on a 2D surface has little or no correlation with their counterpart in 3D [13,25–27].

Traditionally, tumor cell invasion in 3D is studied using a Boyden chamber assay, and these studies have informed us most of what we know about molecular mechanisms in roles of EGF in breast tumor cell invasion [9,14]. For example, PLC γ and PI3K have been identified to affect EGF induced MDA-MB-231 cell invasion using inhibitor studies [10,14,18,19]. One limitation of Boyden chamber is that it provides only population level and endpoint results. Recognizing the importance of cancer cell migration heterogeneity and plasticity, *in vitro* models such as microfluidic models that are compatible with optical imaging and thus single cell analysis have emerged [11,13,15,21]. Recent report from the Lauffenburger lab using microscopic imaging and 3D cell culture showed that EGF increases glioblastoma cell speed through intrinsic signaling pathway and persistence through extrinsic biomatrix cues [21]. In our own labs, we found that EGF enhanced MDA-MB-231 cell speed, although EGF was not a chemoattractant using a 3D microfluidic platform [11].

* Contribution to the Focus Point on “The Physics of Cancer” edited by M. Ben Amar.

** Supplementary material in the form of 4 .mpg and a .pdf files available from the Journal web page at <http://dx.doi.org/10.1140/epjp/i2016-16008-8>

^a e-mail: mw272@cornell.edu

The shape and size of the nuclei of cells have been routinely used as visual cues for diagnosing cancers in the clinical setting rarely has one correlated cancer cell shape and motility types with its invasive state *in vitro*. Animal cell motility within a 3D architecture can be broadly categorized into amoeboid and mesenchymal cell migration [28–32]. Amoeboid cells are mostly rounded in shape and typically form transient and weak adhesion contacts with the biomatrix fibers [31]. To migrate, they send out protrusions into the pores of the biomatrix, and squeeze through the pore structure in a path-finding manner. Leukocytes are mostly amoeboid in shape, and they have been reported to migrate in collagen gel in an integrin independent manner [33]. Mesenchymal cells, on the other hand, are elongated in shape [32,34]. They have bundled or polarized actin filaments, and form long-lived adhesion with the biomatrix fibers. Mesenchymal cells migrate via proteolytic degradation of collagen in an integrin dependent and path-generating manner. Although extensive work has been carried out to study how EGF influences cell speed and persistence, little is known about how EGF impact cell shape and motility phenotypes at single cell level [13,31]. As a result, the roles of EGF in modulating 3D cell migration heterogeneity and plasticity is largely unexplored [35,36].

In this article, we present roles of EGF on the morphology and motility phenotypes of a malignant breast tumor cell line, MDA-MB-231, migrating within a 3D collagen matrix. Our work elucidates the close relation between EGF and cell shape/motility phenotype, suggesting morphological analysis as an alternative approach for characterizing tumor cell invasiveness and metastatic potential.

2 Materials and methods

2.1 3D cell culture

A human malignant breast tumor cell line, MDA-MB-231, was provided by the Center on the Microenvironment and Metastasis at Cornell University. The basal medium for the cell line was DMEM (Invitrogen, Carlsbad, CA), supplemented with 10% FBS (Atlanta Biologicals, Lawrenceville, GA) and antibiotics (100 units penicillin and 100 μg streptomycin, Invitrogen). Cell cultures were maintained every 2–3 days in a T75 flask (Corning, Lowell, MA) with 5–10% of initial confluency (percentage of cell area coverage) within a humidified, CO₂-regulated incubator at 37 °C. EGF (200 $\mu\text{g}/\text{ml}$) were purchased from BD Sciences (Bedford, MA) and stored at –20 °C after reconstitution as instructed by the suppliers. Type I collagen was extracted from rat tails (Pel-Freez, Rogers, AR) and stored at 5 mg/ml in 0.1% acetic acid at 4 °C [11]. Cells from 50–75% confluency from T75 cultures were re-suspended in DMEM with 10% FBS and then mixed at 1×10^6 cells/ml with 1N NaOH (for pH \sim 7), 10X M199 and 1.5 mg/ml collagen on ice. Cell numbers were counted using a hemocytometer (Bright-Line Hemocytometer, Hausser Sci., Horsham, PA).

Previously, we showed that the speed of MDA-MB-231 cells dramatically reduced when the collagen concentrations increased from 1.5 to 3.5 mg/ml [11]. The biomatrix that we recreated is different from *in vivo* biomatrices, which are more complex, more dense, and heterogeneous. But, a high density of collagen is not ideal for *in vitro* assays because the migration of tumor cell is suppressed by the dense and spatially homogenous biomatrix network. Rather, multiphoton imaging of breast tumor cell migration in mouse model shows that fast and persistent tumor cell migration is often associated with three factors —the lack of dense collagen network, amoeboid motion, and the contact of cells with ECM fibers [37,38]. Thus, it is important to place tumor cells in the context of a collagen matrix for *in vitro* studies; processes like tumor cell invasion can be mimicked with close proximity to the *in vivo* situation in such matrices [33,39,40].

2.2 Device design

The main part of the device is a specialized Petri dish (diameter of 3.35 cm) with four divided sections and a 170 μm thin glass bottom (MatTek corp., Ashland, MA) (see fig. 1). Rings of PDMS with an inner diameter of 4 mm, outer diameter of 6 mm and thickness of 400 μm were prepared using biopsy punches. The PDMS rings were then sterilized, and bonded to the bottom of the Petri dish via oxygen plasma treatment (Harrick Plasma Cleaner PDC-001, Harrick Plasma, Ithaca, NY). One PDMS ring was placed in each compartment of the Petri dish. The entire well devices were then treated with oxygen plasma and UV light to ensure sterility. All work was done either inside a biohood or oxygen plasma machine fitted with a sterile air filter. Second, a cell and collagen mixture (5 μl each) was introduced into each of the 4 PDMS wells on ice. Third, the cell embedded collagen within the device was placed in an humidified incubator (5% CO₂, 37 °C) for polymerization, for seven minutes in an inverted position and then thirteen additional minutes in an upright position. Lastly, 500 μl of media with or without EGF was added to each compartment, and the entire assembly was pre-incubated for two hours before being imaged.

We note that a thin (400 μm depth), uniform layer of cell embedded collagen is chosen for the following reasons: 1) thin collagen gels ensure spatial uniformity of the temperature within the collagen during polymerization. It has been shown that the temperature ramping rate during collagen polymerization significantly affects the collagen's fibrous micro-structure and subsequently cellular behavior [41]; 2) thin collagen gels allow cells to access nutrients and chemicals quickly via diffusion; 3) a thin sample improves the optical quality taken with fluorescence and bright field microscopy as collagen is not completely transparent.

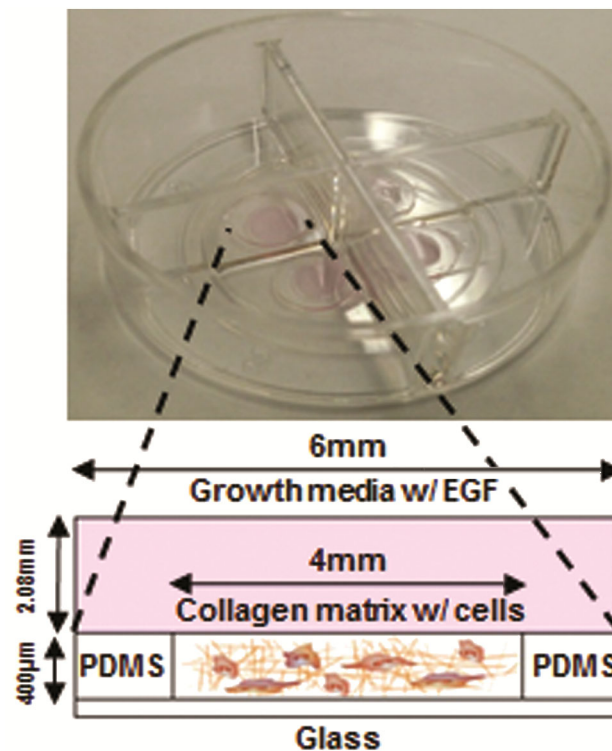


Fig. 1. PDMS well device for MDA-MB-231 cell migration in 3D collagen matrix. An image of the PDMS wells in a Petri dish is presented with the wells filled with growth media. Each Petri dish has 4 subsections, where a PDMS ring is bonded to a glass bottom after oxygen plasma treatment to form a well in each subsection. A cross-sectional view of a single well is depicted with dimensions (drawing is not to scale). Extra 500 μl of growth medium with various EGF concentrations is supplemented in each subsection and the cell cultures are pre-incubated for 2 hours before being imaged, to allow EGF to diffuse through the collagen matrix.

2.3 Imaging and data analysis

For live cell imaging, the device was placed on a microscope stage surrounded by a temperature controlled chamber (Weather Station, Precision Control LLC) set at 37 °C. Within the chamber, the device was surrounded by a smaller Plexiglas chamber set at 37 °C, 100% humidity and 5% CO₂ (CO2-200, In Vivo Scientific, World Precision Instruments, Inc., Sarasota, FL). For each experiment, we imaged 4 wells sequentially using the x - y controlled stage (OptiScan II, Prior Scientific, Inc., Rockland, MA). A set of 4 images was captured every 8 minutes for 16 hours using a bright field microscopy (10X objective, Olympus IX81, Center Valley, PA), and a CCD camera (Orca-ER, Hamamatsu, Bridgewater, NJ). For the data reported here, we imaged one plane close to the center of the cell culture layer in the vertical direction.

Aspect ratio of the cell is used to characterize the cell morphology. Aspect ratio is defined as the ratio of the long and short axis of the ellipse when fitted to the cell shape using ImageJ (NIH) (see fig. 2C). Cell trajectories were obtained using the Manual Tracker in ImageJ from the time series images (see fig. 3). Cell speed U (length of the trajectories divided by time) and persistence length P (displacement of cell trajectory divided by the length of the track) were then computed from the cell trajectories of 16 hour duration (fig. 4A) using an in-house MATLAB program (The MathWorks, Inc., Natick, MA). Here, we define motile cells when $U > 0.2 \mu\text{m}/\text{min}$.

A non-parametric analysis (Mann-Whitney test) was applied between control and experimental groups (EGF) for aspect ratio, persistence length, and normalized speed, while student t-test was used for percentage of mesenchymal cells and percentage of motile cells, using PRISM (GraphPad) (figs. 2 and 4). Linear regression and Pearson correlation was used to determine the correlation between hourly speed, persistence length and aspect ratio using PRISM. After 60 motile cells from each group were randomly selected, hourly speed and the aspect ratio at the end of each hour were obtained. The fastest speed in each aspect ratio range (interval of 0.5) and its corresponding aspect ratio was used for linear regression and Pearson correlation test in each concentration group (fig. 5). The persistence length of 16 hours and the corresponding aspect ratio at the end of time point (16 hours) from the same 60 motile cells from each concentration group was used for linear regression and Pearson correlation test (fig. 6).

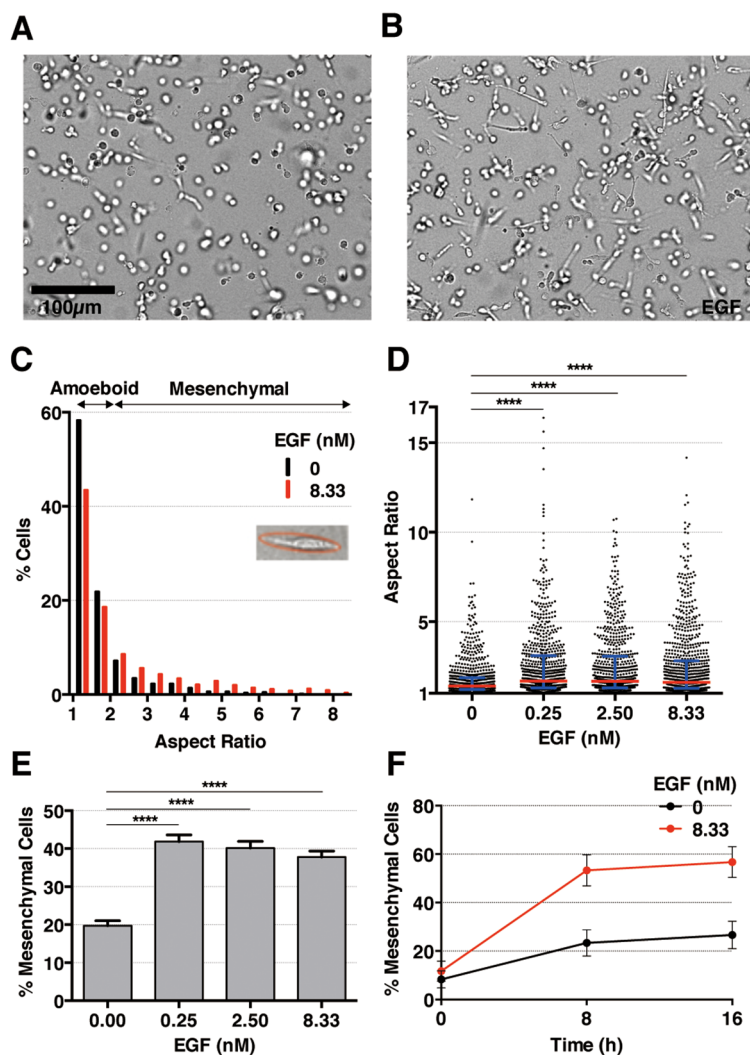


Fig. 2. *EGF promotes mesenchymal cell morphology phenotype.* (A and B) Bright field images of MDA-MB-231 cells embedded in the 3D collagen matrices are displayed for control and 0.25 nM EGF conditions. Both images were taken at the end of the experiment, after 16 hours. (C) The morphology parameter, aspect ratio is obtained after an elliptical fit of each cell as shown. Here we define mesenchymal morphology when cells have aspect ratio larger than 2 and amoeboid morphology when cells have aspect ratio less than 2. Distribution of cell aspect ratio are shown for control and 8.33 nM EGF condition at $t = 16$ hours. (D) Scatter plots of aspect ratio under various EGF conditions at $t = 16$ hours. The differences between median aspect ratio (indicated by the red line) of control group and of EGF conditions are statistically significant. The blue lines represent the 25th and 75th percentiles. (E) Percentage of mesenchymal cells at $t = 16$ hours under various EGF conditions. The differences between percentage of mesenchymal cells of control group and of EGF conditions are statistically significant revealed by student t -test. (F) Time evolution of percentage of mesenchymal cells under control and 8.33 nM EGF condition. All viable cells within each group (2–300 cells) were tracked for plots C–E. Sixty motile cells (cell average speed $> 0.2 \mu\text{m}/\text{min}$) from each group were randomly selected for plot F.

3 Results and discussions

3.1 Exogenous EGF promotes a mesenchymal over amoeboid phenotype of MDA-MB-231

The morphology and migration characteristics of the MDA-MB-231 cells were analyzed using the time sequence images of the cells embedded in collagen taken under control and EGF conditions. For a typical experiment, cells were mixed with collagen supplemented with EGF of various concentrations and placed into 4 PDMS wells (fig. 1), each with a designated EGF concentration, 0, 0.25, 2.50, or 8.33 nM. These concentrations were chosen because the EGFR receptor binding affinity has been reported to have a high value ($K_D = 10\text{--}100 \mu\text{M}$) for a small fraction (2–5%) of the receptors and a low value ($K_D = 2\text{--}5 \text{nM}$) for the majority of the receptors (95–98%), obtained by ^{125}I labeled EGF binding

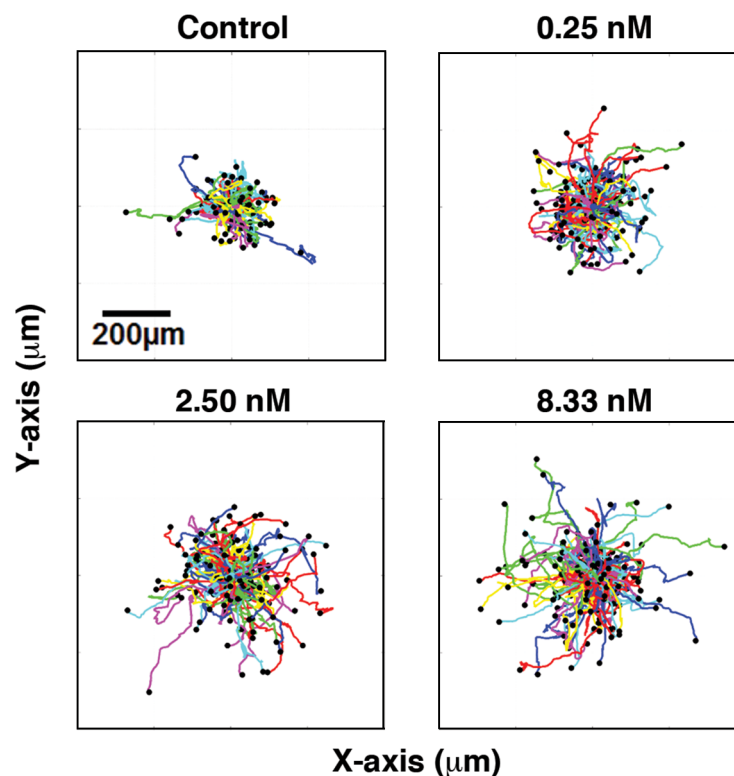


Fig. 3. Polar plots of cell-trajectories under various EGF conditions. Each colored line represents one cell trajectory tracked over 16 hours with an 8 min interval. Each plot contains 150–200 trajectories of motile cells. MDA-MB-231 cells display an increase in dissemination with the increase of exogenous EGF, but no directed cell migration is observed.

assay [42,43]. The initial imaging time, $t = 0$ is defined as the start of the imaging, typically 2 hours after the cells were mixed with collagen. Figures 2A and B shows that MDA-MB-231 cells are more elongated in the presence of EGF in contrast to the ones with no EGF (also in movie SM1 and SM2). The distribution of the cell aspect ratio is skewed towards larger values in the presence of EGF than no EGF (fig. 2C). The median aspect ratio is significantly larger in the presence EGF than no EGF condition (fig. 2D). Aspect ratio of 2.0 was selected as a criterion for defining mesenchymal (> 2.0) and amoeboid cells (< 2.0) to be consistent with previous literature [29,31,44,45]. Using this criterion, the percentage of mesenchymal cells is found to increase significantly in the presence of EGF (fig. 2E) in contrast to the control condition. This is also reflected in the time evolution of the percentage of the mesenchymal cells under control and EGF conditions (fig. 2F).

In current literature, the aspect ratio of 2.0 has been used by a number of groups to define amoeboid (< 2.0) and mesenchymal (> 2.0) cells [29,31,44,45]. This criterion is chosen based on the cell shape, cell migration behavior, actin polarization, focal adhesion complex expression, and RhoA and Rac1 signaling activities. Mesenchymal phenotype is characterized by high signaling activities of Rac1 which leads to the formation of polarized actin bundle, and high expression of focal adhesion complex [34]. They typically migrate via proteolytically degrading biomatrix in a path-generating manner (see the micro-tracks behind the mesenchymal cells in fig. 7 and movie SM3) [46]. In contrast, amoeboid phenotype is characterized by RhoA/ROCK signaling activities, which enhances contractility of cells, allowing them to migrate by squeezing through pores of the ECM. Amoeboid cell motility in leukocytes has been reported to be integrin independent [33]. Typically, cells are rounded in shape, forms weak adhesion contacts with collagen fibers all around the cells, and migrate via a path-finding manner [46] (see movie SM4).

It has been reported that single tumor cells can switch between mesenchymal and amoeboid motility phenotypes under controlled microenvironment [29–31,45]. By blocking pericellular proteolysis, HT-1080 fibrosarcoma and MDA-MB-231 carcinoma cells [31] have been seen to undergo a mesenchymal to amoeboid motility transition. Stiffer collagen I matrix (via adding agarose) has been reported to promote an amoeboid over a mesenchymal cell phenotype in U373-MG glioma cells [30]. Recently, our lab reported that interstitial flows promote an amoeboid over mesenchymal motility in MDA-MB-231 cells [45]. Here, we show that a cytokine, EGF, promotes an amoeboid to mesenchymal motility transition using MDA-MB-231 cells embedded within a 3D collagen matrix. EGF is known to increase the activities of focal adhesion molecules while having minimal impact in changing the physical structure of collagen matrix [47]. In addition, previous research has reported that EGF stimulates the lamellipodia extension in adenocarcinoma cells

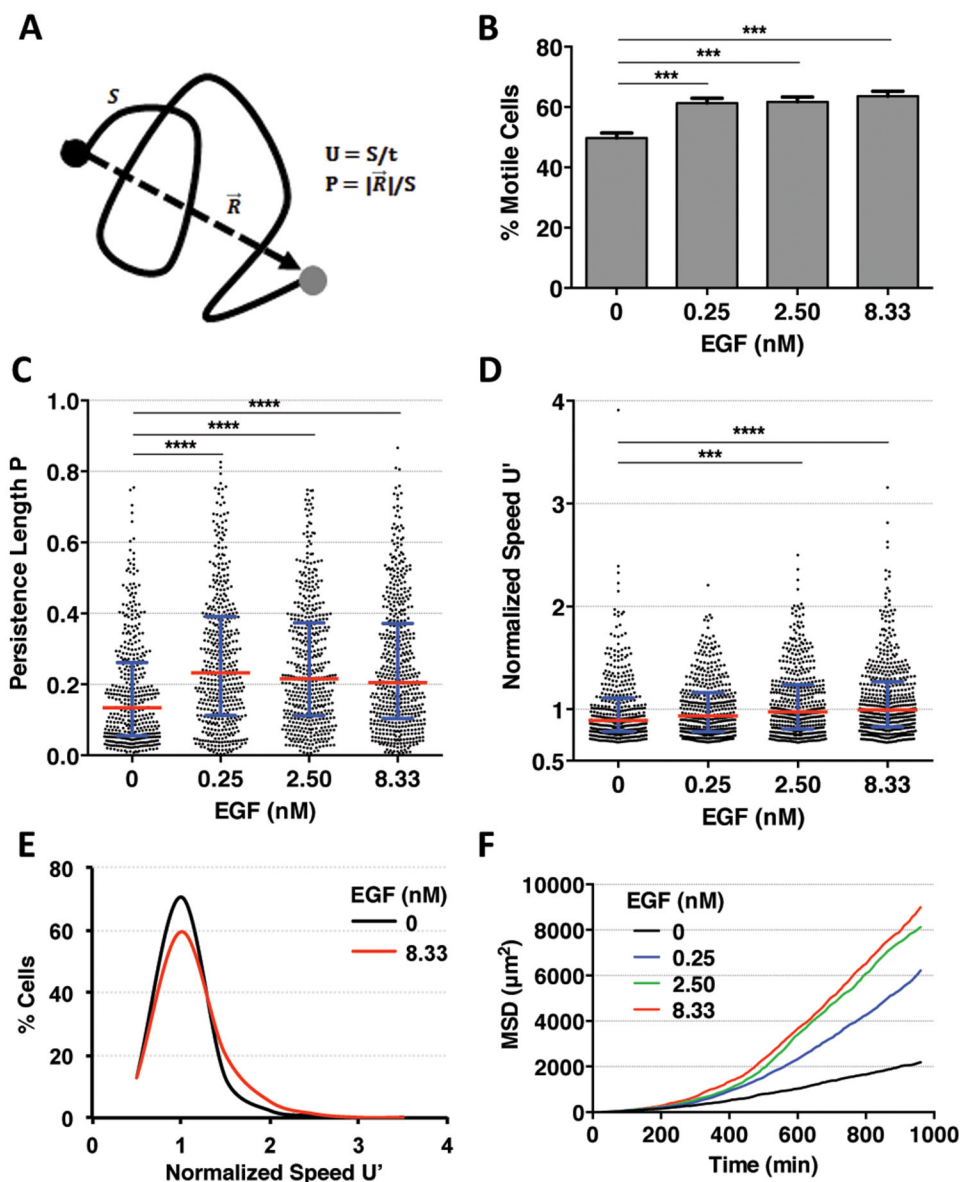


Fig. 4. EGF promotes cell motility and dissemination. (A) Illustration of the migration parameters, average cell speed U and persistence length P . U is calculated by dividing the total length of the cell track (S) by 16 hours, and P is calculated by dividing the net cell displacement by S . (B) Percentage of motile cell in the cell population at $t = 16$ hours for each condition. Exogenous EGF increases percentage of motile cells in the MDA-MB-231 cells with statistical significance in a dose-dependent manner. Student t-test is used. (C and D) Persistence length (C) and normalized speed (D) under various exogenous EGF conditions. EGF increases the median persistence length and speed of the cells. Non-parametric analysis is used, red line is the median and blue lines marks the 25th and 75th percentiles. (E) Distribution of normalized speed for control and EGF condition. (F) Mean squared displacement (MSD) under various EGF conditions. 300–400 motile cells per group are selected for all the above analysis.

by causing accumulation of F-actin and actin polymerization [10,13,17]. Results shown here is consistent with the previous work, in that the enhanced focal adhesion activities due to EGF promote actin polymerization and bundling, which consequently promote mesenchymal cell phenotype in MDA-MB-231 cells.

3.2 EGF increases MDA-MB-231 cell dissemination within a 3D collagen matrix

An important characteristic of tumor cell migration during metastasis is its ability to reach a distant site. Towards this front, we tracked single moving cells using the time series images. Figure 3 depicts single cell trajectories under various EGF conditions. It shows that cells execute random walks under all conditions; however, the presence of EGF enhances cells' ability to spread in a dosage-dependent manner.

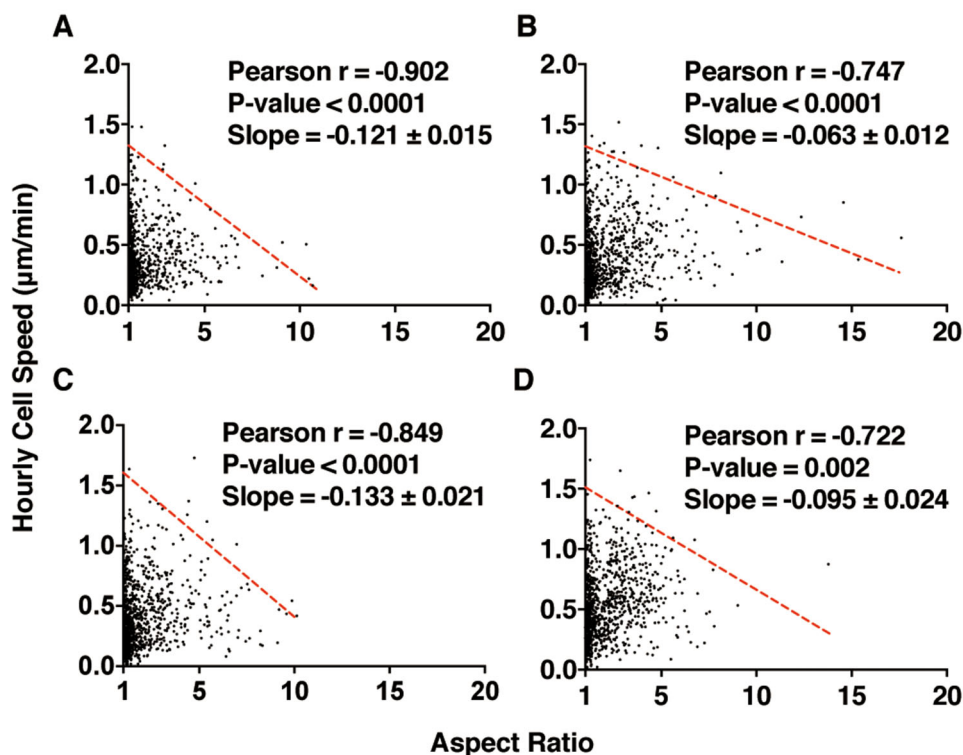


Fig. 5. *The fastest moving cells belong to amoeboid cell phenotype.* Hourly cell speed *versus* aspect ratio for various EGF conditions. Randomly selected 60 motile cells for (A) control, (B) 0.25 nM, (C) 2.50 nM, and (D) 8.33 nM EGF conditions. The red dashed line is a linear fit to the data of maximum speed in a subgroup of cells with aspect ratio bin size of 0.5 *versus* aspect ratio. Both the curve and the Pearson correlation test show that the maximum cell speed of the subgroup decreases with the increases of the aspect ratio. Pearson correlation test is conducted for fastest moving cell in each aspect ratio subgroup of bin size 0.5. *P*-values lower than 0.05 indicates that the test rejects (with 95% confidence) the null-hypothesis that parameters are not correlated. Low *p*-values and correlation coefficient Pearson *r* suggest that the aspect ratio and cell speed are negatively correlated for the fastest cells.

To further quantify cells' ability to disseminate, we computed cell average speed U , persistence length P as well as the mean squared distance (MSD) of the cell population (fig. 4) using the tracks shown in fig. 3. To avoid run-to-run variations, we used the normalized speed after we divided the speed by the average speed from the control group. Figure 4B shows that EGF enhances the percentage of the motile cells ($U \geq 0.2 \mu\text{m}/\text{min}$) within one MDA-MB-231 cell population. Persistence is also augmented with the presence of EGF, with a slight peak at 0.25 nM (fig. 4C). Normalized speed increases with the increase of EGF (figs. 4D and E). Finally, the mean squared displacements (MSD) show that EGF enhances cell dissemination in a dosage dependent manner (fig. 4F).

Our data shows that MDA-MB-231 cells move faster, in a more persistent manner and spread further in the presence of EGF than under the control condition. This is consistent with previous studies [11, 13, 20]. EGF-stimulated cells were reported to have increased motility in a 2D microfluidic device, 3D microfluidic device [11, 15] and multi-well plates [13], in particular with MDA-MB-231 [11, 13, 20]. Similar phenomenon was observed that EGF-stimulated glioblastoma cells had increased speed and persistence compared to non-stimulated cells [21].

We note here that effects of EGF on cell proliferation have been well documented [14, 48]. Interestingly, EGFR-mediated migration and proliferation do not occur simultaneously [49, 50]. In particular, proliferative response to EGF has not been found in MDA-MB-231, although this cell line expresses EGFR [14, 51].

3.3 The fastest moving cells belong to the amoeboid phenotype subgroup and the persistent migrating cells belong to the mesenchymal cell phenotype

To determine if tumor cell motility is correlated with cell morphology, we generated scattered plots of hourly cell speed as a function of cell aspect ratio (fig. 5). Each data point represents an hourly cell speed and the corresponding aspect ratio at the end of that hour. We randomly selected 60 motile cells within each experimental group such that 960 (60×16) data points were generated for each graph in fig. 5. While we did not find a correlation between the

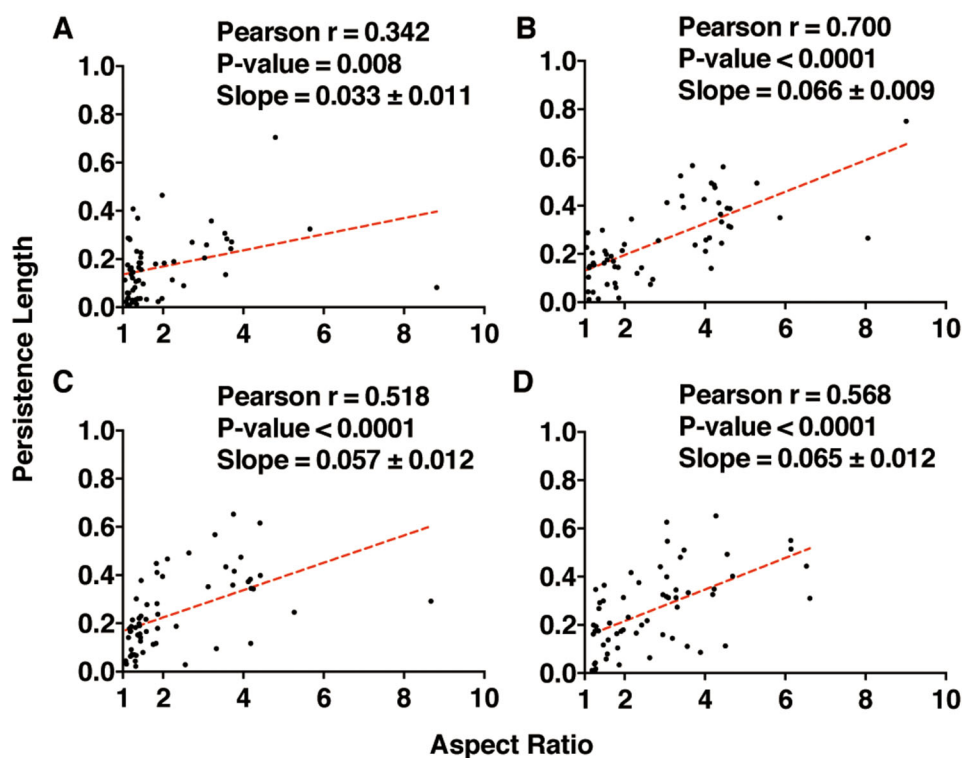


Fig. 6. Persistence length increases with aspect ratio. Pearson correlation test between persistence length and aspect ratio is applied for the same randomly-selected motile 60 cells in fig. 5 for (A) control, (B) 0.25 nM, (C) 2.50 nM, and (D) 8.33 nM EGF conditions. The red dashed line is a linear fit to all the data points. The low p -values indicate that all tests accept the alternative hypothesis that P and aspect ratio are correlated. Pearson r value of 0.3–0.5 indicates positive correlation, and 0.5–1.0 indicates strong positive correlation between observed parameters. The correlation coefficients for P and aspect ratio suggest an overall positive correlation.

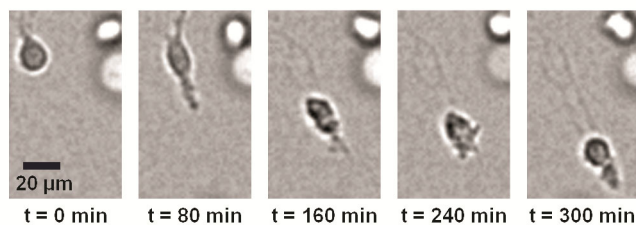


Fig. 7. Characteristic path-generation in a 3D biomatrix when a cell migrates in a mesenchymal mode. A cell migrates in a mesenchymal mode leaves a path in a 3D biomatrix.

aspect ratio and the speed for entire population, fig. 5 shows that the maximum speed within each aspect ratio bin is inversely correlated with the aspect ratio. The red dashed lines are fits to the curve of maximum speed of the aspect ratio subgroup (bin size 0.5) versus aspect ratio. A negative slope (ranging from -0.06 to -0.133) is clearly seen for both control and EGF conditions. In addition, Pearson correlation test using the maximum speed of each aspect ratio subgroup also supports the conclusion that the maximum speed of the subgroup decreases with the aspect ratio. The obtained Pearson r values ranging from -0.7 to -0.9 imply a strong negative-linear correlation between two parameters and the resulting maximum p -value of 0.002 mean that the null hypothesis of no correlation is rejected with over 99.8% confidence in all four cases. This result demonstrates that the fastest moving cells belong to subgroup of amoeboid type.

The scattered plot of persistence length versus aspect ratio suggests that persistence length increases with aspect ratio (fig. 6). We used the same 60 randomly selected motile cells from each EGF concentration group in fig. 5. Due to the nature of persistence length, we used persistence length for 16 hours and its corresponding aspect ratio at 16 hours. This result implies that mesenchymal cells move more persistently than amoeboid cells. This interpretation is in accordance with the fact that amoeboid cells move via sending protrusions into the biomatrix pores in a path-finding manner, while mesenchymal cells migrate along the biomatrix fiber in a path-generating way [30]. When the data were fitted to a linear function (red dashed line), the results show that persistence length and the aspect ratio are

positively correlated with positive slope values. This is further confirmed with the Pearson correlation test: positive Pearson r values ranging 0.3–0.7 imply that there is a positive correlation between two parameters and the resulting maximum p -value of 0.008 means that the null hypothesis of no correlation is rejected with over 99.2% confidence in all 4 cases. This result shows that mesenchymal cells migrate more persistently than amoeboid cells. We note that the persistence length is different from the persistence time in the persistence random walk model. Yet, our result supports the previous study between persistence time and EGF supplementation [13].

The results shown here demonstrate the advantage of live cell imaging data analysis, which allows us to interrogate cancer cell heterogeneity and plasticity at single cell or sub-population level. Our results show that the fastest moving cells belong to the sub-population of amoeboid cells, while the persistent cells belong to the sub-population of mesenchymal cells. It is interesting to note that although the average speed of the entire cell population increases with the EGF concentration and EGF promotes mesenchymal over amoeboid motility, we find that the fastest moving cells always belong to the amoeboid cell phenotype. We emphasize the importance of single cell analysis because heterogeneity and plasticity are hallmarks of cancer, and results from population level analysis may mask important messages that can only be revealed using single cell or sub-population level analysis.

4 Conclusions and future perspectives

Tumor cell motility behavior is heterogenetic and plastic, and it is critically regulated by its dynamic microenvironment. It is thus important to investigate tumor cell migration both in time and at single cell level. In this article, we demonstrate that EGF promotes a mesenchymal over amoeboid cell motility phenotype using breast tumor cell line, MDA-MB-231. In addition, EGF enhances cell dissemination within 3D collagen matrix via the increase of the persistence length and speed. The direct correlation between the persistence and the aspect ratio indicates that EGF may increase persistence via promoting mesenchymal cell phenotype. This work highlights the importance of physical parameters in revealing cell invasive phenotype, suggesting that cell aspect ratio can potentially be an important biomarker for diagnose of cancer cell invasiveness in the near future.

As 3D cell migration becomes mainstream, a number of novel motility mechanism including collective cell migration have been reported in the current literature [28, 29, 32, 35, 36, 44]. The question of motility mode switch may be more frequent in tumor cells than other cell types because tumor cells are known to be plastic and heterogenic. A number of interesting questions arising: i) whether/how tumor plasticity correlates with tumor metastatic potential; ii) whether/how biomatrix network density and cytokines synergistically influence tumor cell invasion phenotype. A drug cocktail, a combination of drugs blocking multiple migration types, has been proposed by Sahai and Marshall [28]. The use of MMP inhibitors and Rho-ROCK inhibitors significantly reduced tumor cell invasion [28]. Due to the redundancy and compensation mechanism at molecular level [52], the shape and motility phenotype analysis presented here provides a novel entry point for finding key intracellular signaling molecules that control tumor cell invasion.

This work was supported by the National Cancer Institute (R21CA138366, R21RR025801), and the Cornell Center on the Microenvironment & Metastasis, a Physical Sciences Oncology Center (U54CA143876).

Author contribution statement

Dongil T. Geum and Beum Jun Kim contributed equally to this work.

References

1. B.D. Harms, G.M. Bassi, A.R. Horwitz, D.A. Lauffenburger, *Biophys. J.* **88**, 1479 (2005).
2. G. Fontanini, S. Vignati, D. Bigini, A. Mussi, H. Lucchi, C.A. Angeletti, R. Pingitore, S. Pepe, F. Basolo, G. Bevilacqua, *Eur. J. Cancer* **31A**, 178 (1995).
3. R.N. Jorissen, F. Walker, N. Pouliot, T.P.J. Garrett, C.W. Ward, A.W. Burgess, *Exp. Cell Res.* **284**, 31 (2003).
4. L.J. McCawley, P. O'Brien, L.G. Hudson, *Endocrinology* **138**, 121 (1997).
5. T. Turner, P. Chen, L.J. Goodly, A. Wells, *Clin. Exp. Metastas.* **14**, 409 (1996).
6. B.S. Verbeek, S.S. Adriaansen-Slot, T.M. Vroom, T. Beckers, G. Rijksen, *Febs. Lett.* **425**, 145 (1998).
7. A. Wells, J. Kassis, J. Solava, T. Turner, D.A. Lauffenburger, *Acta Oncol.* **41**, 124 (2002).
8. M.F. Ware, A. Wells, D.A. Lauffenburger, *J. Cell Sci.* **111**, 2423 (1998).
9. S. Hart, O.M. Fischer, N. Prenzel, E. Zwick-Wallasch, M. Schneider, L. Hennighausen, A. Ullrich, *Biol. Chem.* **386**, 845 (2005).
10. Q. Huang, H.M. Shen, C.N. Ong, *Cell. Mol. Life Sci.* **62**, 1167 (2005).
11. B.J. Kim, P. Hannanta-Anan, M. Chau, Y.S. Kim, M.A. Swartz, M.M. Wu, *Plos One* **8**, e68422 (2013).
12. J.S. Krueger, V.G. Keshamouni, N. Atanaskova, K.B. Reddy, *Oncogene* **20**, 4209 (2001).

13. A.S. Meyer, S.K. Hughes-Alford, J.E. Kay, A. Castillo, A. Wells, F.B. Gertler, D.A. Lauffenburger, *J. Cell. Biol.* **197**, 721 (2012).
14. J.T. Price, T. Tiganis, A. Agarwal, D. Djakiew, E.W. Thompson, *Cancer Res.* **59**, 5475 (1999).
15. W.K. Raja, B. Gligorijevic, J. Wyckoff, J.S. Condeelis, J. Castracane, *Integr. Biol. Quantit. Biosci. nano macro* **2**, 696 (2010).
16. C. Sawyer, J. Sturge, D.C. Bennett, M.J. O'Hare, W.E. Allen, J. Bain, G.E. Jones, B. Vanhaesebroeck, *Cancer Res.* **63**, 1667 (2003).
17. J.E. Segall, S. Tyrech, L. Boselli, S. Masseling, J. Helft, A. Chan, J. Jones, J. Condeelis, *Clin. Exp. Metastas.* **14**, 61 (1996).
18. J. Sturge, J. Hamelin, G.E. Jones, *J. Cell. Sci.* **115**, 699 (2002).
19. R.H. Sun, P. Gao, L. Chen, D.L. Ma, J.M. Wang, J.J. Oppenheim, N. Zhang, *Cancer Res.* **65**, 1433 (2005).
20. S.J. Wang, W. Saadi, F. Lin, C.M.C. Nguyen, N.L. Jeon, *Exp. Cell. Res.* **300**, 180 (2004).
21. H.D. Kim, T.W. Guo, A.P. Wu, A. Wells, F.B. Gertler, D.A. Lauffenburger, *Mol. Biol. Cell.* **19**, 4249 (2008).
22. D.A. Lauffenburger, A.F. Horwitz, *Cell* **84**, 359 (1996).
23. G. Carpenter, in *The EGF Receptor Family*, edited by G. Carpenter (Academic Press, Burlington, 2003) pp. 69.
24. J.L. Tan, J. Tien, D.M. Pirone, D.S. Gray, K. Bhadriraju, C.S. Chen, *Proc. Natl. Acad. Sci.* **100**, 1484 (2003).
25. Stephanie S. Chang, W.-H. Guo, Y. Kim, Y.-L. Wang, *Biophys. J.* **104**, 313 (2013).
26. E. Cukierman, R. Pankov, D.R. Stevens, K.M. Yamada, *Science* **294**, 1708 (2001).
27. L.G. Griffith, M.A. Swartz, *Nat. Rev. Mol. Cell. Biol.* **7**, 211 (2006).
28. E. Sahai, C.J. Marshall, *Nat. Cell. Biol.* **5**, 711 (2003).
29. V. Sanz-Moreno, G. Gadea, J. Ahn, H. Paterson, P. Marra, S. Pinner, E. Sahai, C.J. Marshall, *Cell* **135**, 510 (2008).
30. T.A. Ulrich, A. Jain, K. Tanner, J.L. MacKay, S. Kumar, *Biomaterials* **31**, 1875 (2010).
31. K. Wolf, I. Mazo, H. Leung, K. Engelke, U.H. von Andrian, E.I. Deryugina, A.Y. Strongin, E.B. Brocker, P. Friedl, *J. Cell. Biol.* **160**, 267 (2003).
32. D. Yamazaki, S. Kurisu, T. Takenawa, *Oncogene* **28**, 1570 (2009).
33. T. Lammermann, B.L. Bader, S.J. Monkley, T. Worbs, R. Wedlich-Soldner, K. Hirsch, M. Keller, R. Forster, D.R. Critchley, R. Fassler *et al.*, *Nature* **453**, 51 (2008).
34. K. Pankova, D. Rosel, M. Novotny, J. Brabek, *Cell. Mol. Life Sci.* **67**, 63 (2010).
35. P. Friedl, J. Locker, E. Sahai, J.E. Segall, *Nat. Cell. Biol.* **14**, 777 (2012).
36. P. Friedl, K. Wolf, *J. Cell Biol.* **188**, 11 (2010).
37. J. Condeelis, J.E. Segall, *Nat. Rev. Cancer* **3**, 921 (2003).
38. W.G. Wang, J.B. Wyckoff, V.C. Frohlich, Y. Olynykov, S. Huttelmaier, J. Zavadil, L. Cermak, E.P. Bottinger, R.H. Singer, J.G. White *et al.*, *Cancer Res.* **62**, 6278 (2002).
39. U. Haessler, M. Pisano, M.M. Wu, M.A. Swartz, *Proc. Natl. Acad. Sci. U.S.A.* **108**, 5614 (2011).
40. U. Haessler, J.C.M. Teo, D. Foretay, P. Renaud, M.A. Swartz, *Integr. Biol.* **4**, 401 (2012).
41. M.S. Hall, R. Long, X. Feng, Y. Huang, C.Y. Hui, M. Wu, *Exp. Cell. Res.* **319**, 2396 (2013).
42. J. Schlessinger, *J. Cell. Biol.* **103**, 2067 (1986).
43. J. Schlessinger, *Biochemistry-U.S.* **27**, 3119 (1988).
44. R.J. Petrie, N. Gavara, R.S. Chadwick, K.M. Yamada, *J. Cell. Biol.* **197**, 439 (2012).
45. Y.L. Huang, C.-K. Tung, A. Zheng, B.J. Kim, M. Wu, *Integr. Biol.* **7**, 1402 (2015).
46. M.L. Taddei, E. Giannoni, A. Morandi, L. Ippolito, M. Ramazzotti, M. Callari, P. Gandellini, P. Chiarugi, *Cell. Commun. Signal* **12**, 24 (2014).
47. Y.F. Yang, Y.N. Zhao, B. Chen, Q.Q. Han, W.J. Sun, Z.F. Xiao, J.W. Dai, *Tissue Eng. A* **15**, 3589 (2009).
48. E.T. Roussos, J.S. Condeelis, A. Patsialou, *Nat. Rev. Cancer* **11**, 573 (2011).
49. A. Wells, *Int. J. Biochem. Cell. B* **31**, 637 (1999).
50. A.K.V. Iyer, K.T. Tran, L. Griffith, A. Wells, *J. Cell. Physiol.* **214**, 504 (2008).
51. N.E. Davidson, E.P. Gelmann, M.E. Lippman, R.B. Dickson, *Mol. Endocrinol.* **1**, 216 (1987).
52. A. Wells, J. Grahovac, S. Wheeler, B. Ma, D. Lauffenburger, *Trends Pharmacol. Sci.* **34**, 283 (2013).